Chapter 3

Enhancing the energy storage capacity of PVDF-based nanocomposite with the help of hydroxylated V_2O_5 as filler

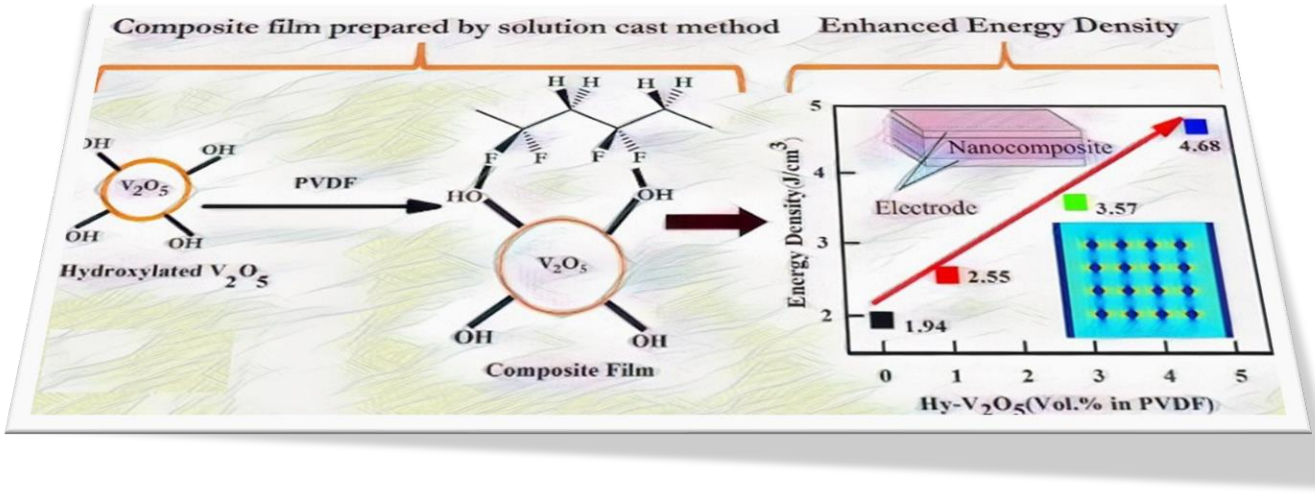

Chapter 3: Enhancing the energy storage capacity of PVDF-based nanocomposite with the help of hydroxylated V_2O_5 as filler

3.1 Introduction

As we have discussed in the chapter 1, the dielectric properties and energy storage of the nanocomposite have been greatly improved by the ceramic nonconducting dielectric filler reinforcement in the PVDF matrix. However, to achieve the required enhancement, a higher amount of such filler loading is required, which leads to a trade-off between the dielectric properties and breakdown strength of the nanocomposite. To circumvent the trade-off between the dielectric properties and breakdown strength, the conducting filler can be used in PVDF matrix, to achieve desired storage and dielectric properties as the conducting filler in low concentration can better improve dielectric constant in comparison to nonconducting filler[24,25]. Various types of semiconducting and conducting materials have been used as filler in PVDF matrix. Cao et. al. synthesized the TiO_x nanoparticles and incorporated in PVDF which resulted enhancement in the energy density to 7.43 J/cm^3 with energy efficiency ~55%. However, the efficiency is moderate at high electric field (4800 kV/cm)[10]. The PVDF/Mxene nanocomposite was synthesized by Feng et. al. and the energy density was achieved to be 2.5 J cm^{-3} with the good efficiency of ~64% [89]. Furthermore, semiconducting ferrites hydroxylated-$BiFeO_3$ [73], hydroxylated $LaFeO_3$[90] and $GdFeO_3$ [90] have also been used as filler to synthesize the PVDF nanocomposites to enhance the dielectric properties. Thus, conducting and semiconducting nanofillers have shown considerable promise to enhance the storage properties of the PVDF

based nanocomposites that are potentially applicable in advance technologies such as actuators, transducers, memory devices and high energy density capacitors [91,92]. In view of this, we have selected semiconducting V_2O_5 as the filler material to enhance the dielectric energy storage properties of PVDF. The V_2O_5 is generally n-type semiconductor which can be transformed to p-type when hydroxylated and thus may act as proton conducting medium[93]. In 1980, researchers have shown that V_2O_5 is ferroelectric as well[94]. Thus, V_2O_5 being a semiconducting material with ferroelectricity can be a highly suitable filler to incorporate in the PVDF matrix to get desirable properties.

In this chapter, we have demonstrated the synthesis and characterizations of PVDF based nanocomposite, with the semiconducting V_2O_5 filler after treating it with H_2O_2 as a refluxing agent, to make a better nanocomposite. We have taken varying volume % of the filler with the 1vol%, 3vol%, 5vol% and 8vol% in the PVDF matrix. The nanocomposite film with the 8vol% of the filler loading was only subjected to characterized with PE loop but the values of the polarization are not promising due to percolation threshold as described in the Chapter 1. Structural and morphological studies have been done to know the formation of the electroactive phase and a stable self-standing film. The dielectric properties are studied in detail. The energy density and breakdown strength are calculated with the help of a hysteresis loop and Weibull analysis.

3.2 Synthesis of Hy-V_2O_5, PVDF/ Hy-V_2O_5 nanocomposite films

The thick films of PVDF/Hy-V_2O_5 nanocomposites were prepared by solution cast method. N, N-Dimethylformamide (DMF) was used as solvent for the preparation of thick film. The PVDF was dissolved homogeneously in DMF solvent using magnetic stirring for 1 hour. The as received V_2O_5 powder was further crushed into fine powders to reduce the particle size with help of high energy ball mill under ethanol medium using PM400MA, RETSCH, Gmbh, Germany. The milled powder was dried, and then hydroxylated using H_2O_2 (30%v/v) for 6

hours at 105°C temperatures. The hydroxylated V_2O_5 powder was dried at 120 °C and then dispersed in DMF solvent by ultrasonicating for 15 minutes with the help of probe sonicator, followed by stirring for another 1 hour. The obtained dispersion of Hy-V_2O_5 in DMF was poured into already prepared PVDF solution and kept for 7 hours magnetic stirring at 50°C. The obtained mixture was further ultrasonicated for 15 minutes and poured in on a petri dish and kept in oven at 110°C for the whole night to get the nanocomposite film after drying. The whole synthesis process is shown schematically in Figure 3.1.

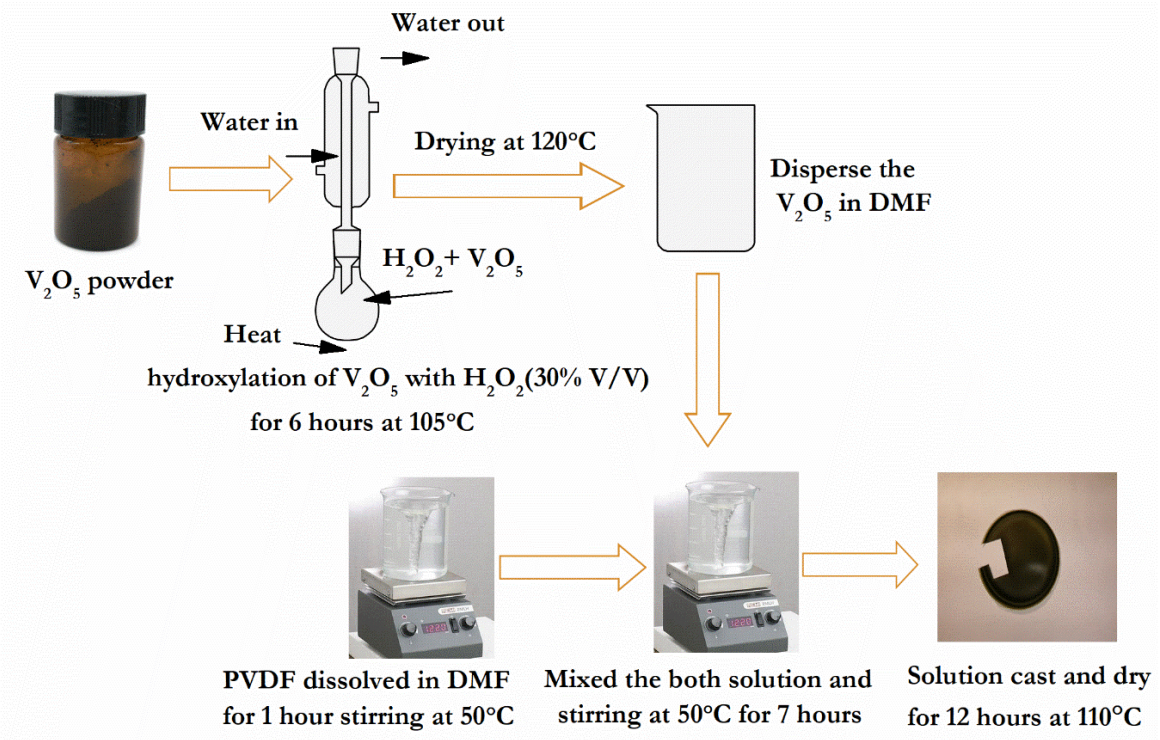

Figure 3.1. The scheme of preparation of thick film of PVDF and PVDF/Hy-V_2O_5 composites.

3.3 Results and discussion

3.3.1 UV-Visible spectra and Tauc's plot of Hy-V_2O_5

The optical band gap of materials can be calculated with the help of the UV-Vis spectra using the formula: $\boldsymbol{\alpha h\nu = B(h\nu - E_g)^n}$, where hν is the incident photon energy, B is the edge width

parameter and n [= 1/2 (direct allowed), 3/2 (direct forbidden), 2 (indirect allowed), 3 (indirect forbidden transitions)] is the exponent which can have values depending on the type of electronic transition causing the absorption [95,96]. So, the band gap of Hy-V_2O_5 is calculated with the help of UV-Vis spectra by plotting the Tauc's plots given by the equation $(\alpha h\nu)^{1/n}$ **vs** $h\nu$ as shown in Figure 3.2, by extrapolating a straight line in the linear region of the plot to zero ($\alpha = 0$). The calculated values of direct forbidden and indirect allowed bands are found to be (2.16 ± 0.04) eV and (2.03 ± 0.04) eV, respectively for nano Hy-V_2O_5 as shown in Figure 3.2. A similar method has also been adopted earlier for the estimations of direct forbidden and indirect allowed bands for V_2O_5 [96].

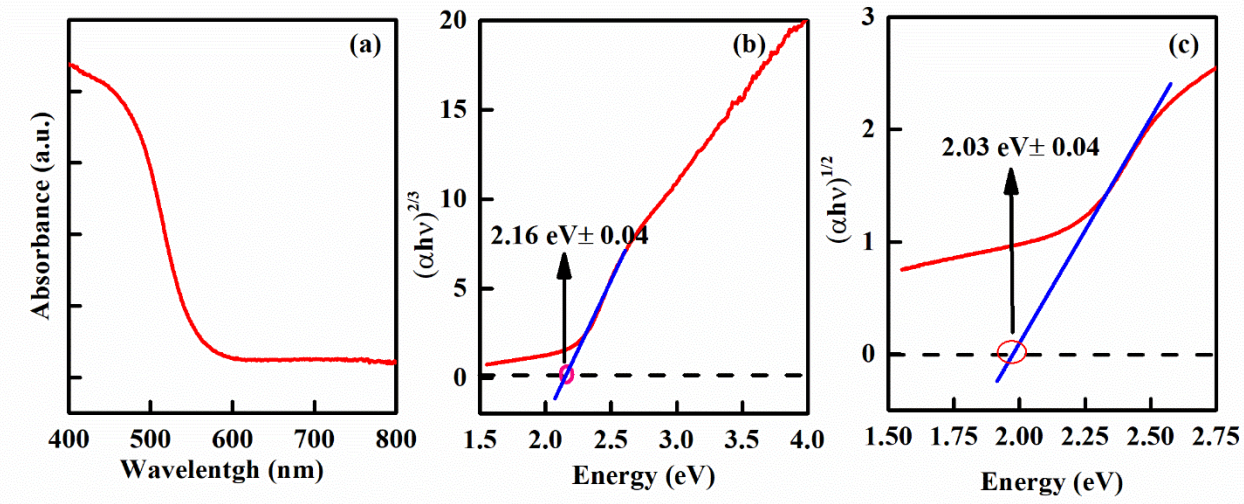

Figure 3.2. (a) UV-Vis spectra, band gap for (b) direct forbidden and (c) indirect allowed transition, using Tauc's plot for Hydroxylated V_2O_5.

3.3.2 X-Ray diffraction pattern analysis

X-Ray diffraction (XRD) analysis was performed to know crystalline nature of pure PVDF and PVDF/Hy-V_2O_5 nanocomposite films. The XRD pattern of the PVDF powder Purchased is have purely α-phase and after processing PVDF powder to PVDF film, the high intensity peaks of α-, β- and γ-phases present at 2θ corresponding to the 18.4°, 26.5; 20.6°, 36.1° and 18.5°, 20.3°, 39.4°, respectively, are observed, as shown in Figure 3.3 (a), that means

film is having electroactive phase is dominance [12,97]. From the previous literatures reports, the PVDF film developed by solution cast method in the solvent N,N-Dimethyl formamide at a temperature of 100℃ shows the presence of α-, β- and γ-phase [98]. The PVDF film shows semi-crystalline nature. As the content of Hy-V_2O_5 filler is increased from 1% v/v to 5%v/v, the XRD peaks of Hy-V_2O_5 dominates over the peaks of PVDF. Analysis of the XRD patterns of V_2O_5 nano milled powder was done with the help of X'Pert high score software, it has been found that the crystal structure of V_2O_5 is orthorhombic and well matches with the JCPDS file no.41-1426 as shown in the Figure 3.3.

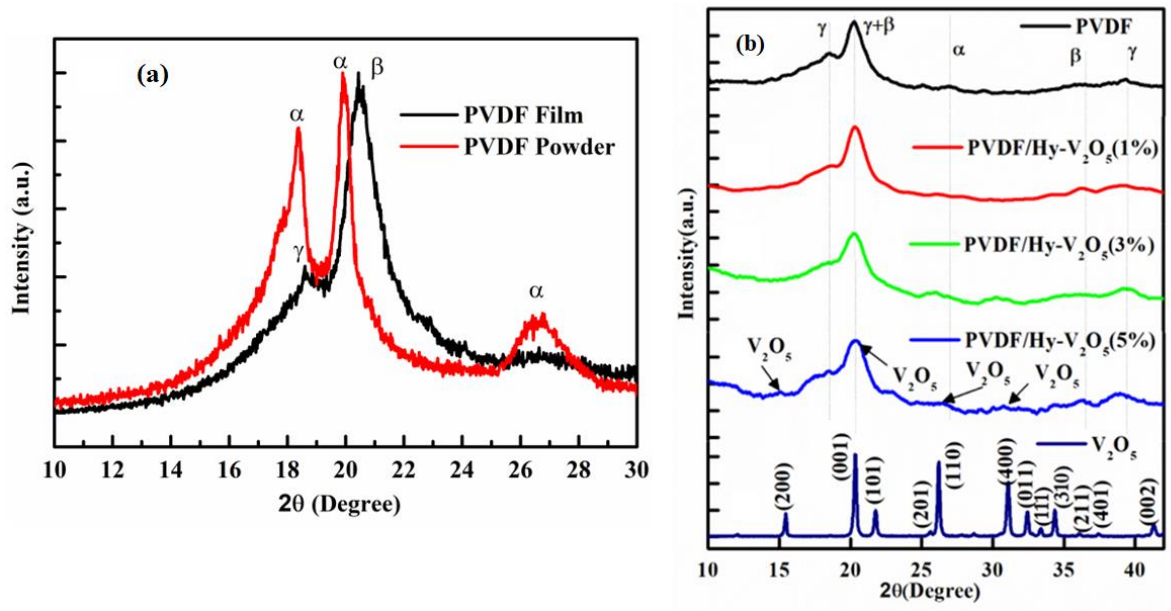

Figure 3.3 XRD patterns comparison of (a) neat PVDF powder and PVDF film and (b) PVDF film and PVDF/Hy-V_2O_5 nanocomposites thick films.

3.3.3 Fourier-transform infrared spectroscopy (FTIR) Analysis and

In Figure 3.4(a), the FTIR spectrum shows the hydroxylation of V_2O_5 as O-H peaks can be seen at 3435 cm^{-1}, 1635 cm^{-1} and 1386 cm^{-1}. Further the stretching band of V=O and V-O-V are at 1004 cm^{-1} and (476 cm^{-1}, 788 cm^{-1}), respectively [99]. In the FTIR spectrum, absorption peaks of PVDF having α-, β- and γ-phases can be categorized in the three categories: (1) peaks present in all phases can be known as common peaks; (2) peaks at those position which are

exclusive peaks for the particular phase; and (3) peaks present only in two different phases which can be called as dual peaks [100]. The FTIR spectrum of PVDF have common peaks in the range of 876–885 cm^{-1}, 1067–1075 cm^{-1}, 1171-1182 cm^{-1} and 1398–1404 cm^{-1} [34,101]. Specific crystalline phases are identified by the exclusive peaks. Exclusive peaks at 410 cm^{-1}, 489 cm^{-1}, 614 cm^{-1}, 763 cm^{-1}, 795 cm^{-1}, 854 cm^{-1}, 975 cm^{-1}, 1149 cm^{-1}, 1209 cm^{-1}, 1383 cm^{-1} and 1423 cm^{-1} are referred to α-phase of PVDF as shown in Figure 3.4(b). For β-phase, the exclusive peaks are present at the positions 445 cm^{-1}, 473 cm^{-1} and 1275 cm^{-1} and the exclusive peaks for the γ-phase are located at the positions 431 cm^{-1}, 482 cm^{-1}, 811 cm^{-1} and 1234 cm^{-1} as shown in Figure 3.4(b) [102]. The α-phase has less strong absorbance in comparison to β-, γ-phases, so the two peaks at around 840 cm^{-1}, 510 cm^{-1} are used to characterize the electroactive β-phase or γ- phases or both. The β, γ-phases also have peaks at 1428-1432 cm^{-1} [100,102]. The high temperature crystallization of γ-phase is exclusively assigned to the 776 cm^{-1} and 833 cm^{-1} bands [92]. Based on exclusive peaks at the bands at around 614 cm^{-1}, 1275 cm^{-1}, and 1234 cm^{-1}, different phases like α, β and γ can be identified and differentiated.

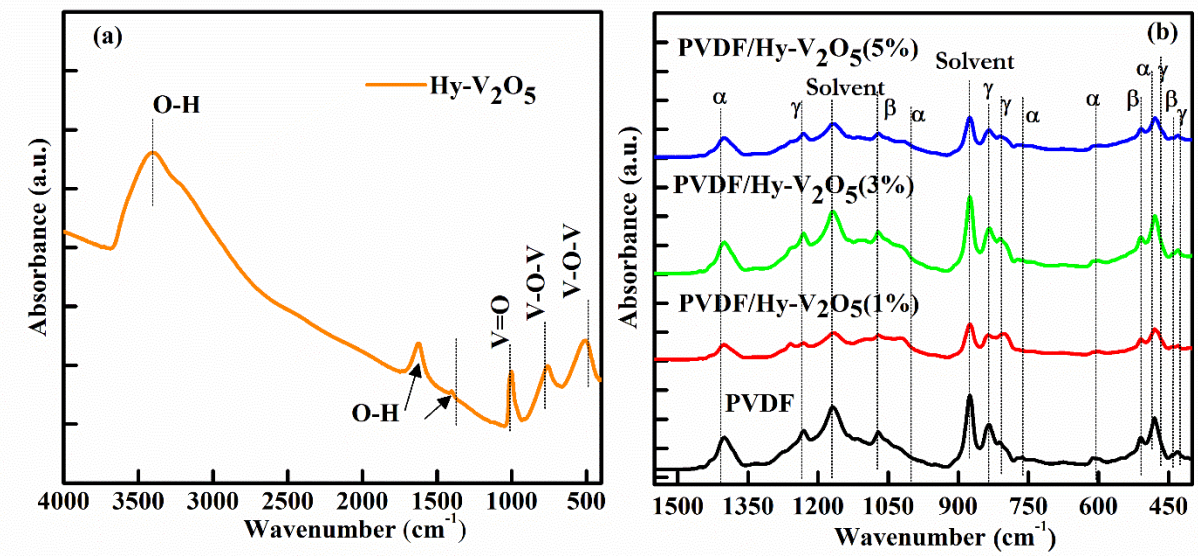

Figure 3.4. FTIR Spectra of **(a)** Hy-V_2O_5, (b) Pure PVDF and its nanocomposites with different filler volume percentage.

3.3.4 X-ray photoelectron spectroscopy (XPS) analysis

XPS analysis of PVDF and PVDF/Hy-V_2O_5 (5%) was done to ascertain the composition (see Figure 3.5 (a-d)). There was no significant difference in the peak positions of the XPS spectra for PVDF and PVDF/Hy-V_2O_5 (5%). Because of the lower amount of loading of Hy-V_2O_5, we cannot clearly see the peaks of Hy-V_2O_5 in the XPS survey full scan (Figure 3.4(a)), but we can see the presence of the nanofiller in the PVDF nanocomposite separately as shown in Figure 3.5(b). The V2p peaks can be allotted as $V2p_{3/2}$ and $V2p_{1/2}$, the $V2p_{3/2}$ is divided into two position of binding energies 516.1 eV and 517.3 eV showing the presence of V^{4+} and V^{5+} respectively[103]. F1s peak is located at 687.5 eV and shows minor deviation in nanocomposite that may be due to surface interfacial interaction of PVDF backbone and Hy-V_2O_5 [104–106]. Further, as shown in the Figure 3.4(d), the C1s spectrum of PVDF and PVDF/Hy-V_2O_5 (5%) shows two major peaks at 290.9 eV and 286.6 eV which are attributed to -CF_2 and -CH_2 of PVDF backbone (-CH_2-CF_2-), respectively, along with a shoulder peak of -C_xH_y- at 284.6 eV [104–106].

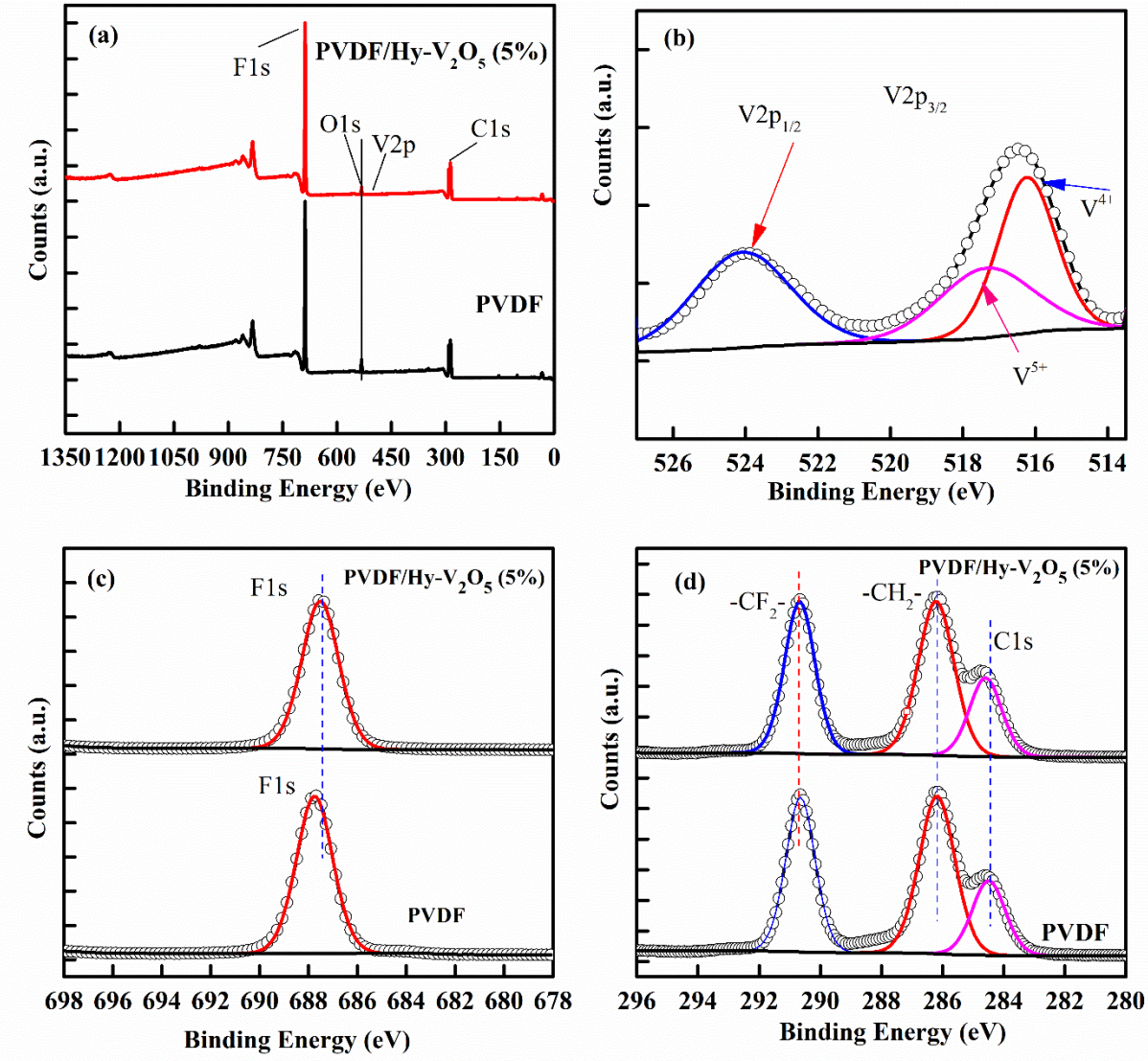

Figure 3.5 (a) XPS survey of PVDF, PVDF/Hy-V_2O_5 (5%), (b) $V2p_{3/2}$ and $V2p_{1/2}$, (c) F1s of PVDF, PVDF/Hy-V_2O_5 (5%), (d) C1s component of XPS spectra of PVDF, PVDF/Hy-V_2O_5 (5%).

3.3.5 Thermal Analysis using DSC-TGA

To get the idea of thermal stability, crystalline nature and mass loss of PVDF/Hy-V_2O_5 nanocomposites, we have used the thermogravimetric analysis (TGA). Differential scanning calorimetry (DSC) has been used for getting idea of energy absorption or release, while heating or cooling the sample. Figure 3.6(a) shows the DSC endothermic heating peak at around 168 °C in all the compositions, the area under this peak represents the degree of crystallinity. The degree of crystallinity can be calculated using the equation (1) given below [107]:

$$\Delta X_c = \frac{\Delta H_f}{(1-\emptyset)\Delta H_f^o} \times 100 \quad (3.1)$$

where, ΔH_f is the fusion heat of the sample and ΔH_f^o is the fusion heat of 100% crystalline PVDF that is 103.40 J/g [108], $\emptyset$ is the % weight of reinforcing ceramic (Hy-V_2O_5) in polymer matrix. Due to increased dipole interaction, electroactive phase (β, γ -phase) coherence energy is higher, α -phase endothermic melting (T_m) is lower than the endothermic peak of the β-phase as shown in Figure 3.6(a). The 1.2 °C change in T_m is related to the increase in electroactive phase. However, the loading of low amount (1 vol% and 3 vol%) of filler, in PVDF may have little or no impact. The calculated value of crystallinity using equation 1 for the pure PVDF ($\Delta X_c = 23.02\%$) is less than that of PVDF/Hy-V_2O_5 (5%) ($\Delta X_c = 36.45\%$). The small deviation at ~120°C and 137°C in the PVDF/Hy-V_2O_5 (5%) DSC plot is due to the transition of V_2O_5 during heating of nanocomposite film that is shown by the red dotted line in Figure 3.5(a) [109] . There was no weight loss in the TGA plot up to 450 °C temperatures in the process, and after that, it can be seen in Figure 3.6(b) that steep declination occurs, which represents the mass loss of around 53%. The TGA result of our sample was found to be identical to the previous results for the PVDF-based nanocomposites [110]. With this, we can conclude that in the range of 450 °C to 520 °C, endothermic process is taking place which helps in dissociating the ceramic filler from the polymer matrix. This endothermic process is known as pyrolysis. The TGA curve does not show any change between 160 and 180 °C, therefore we may infer that PVDF is stable with nanofiller in this range.

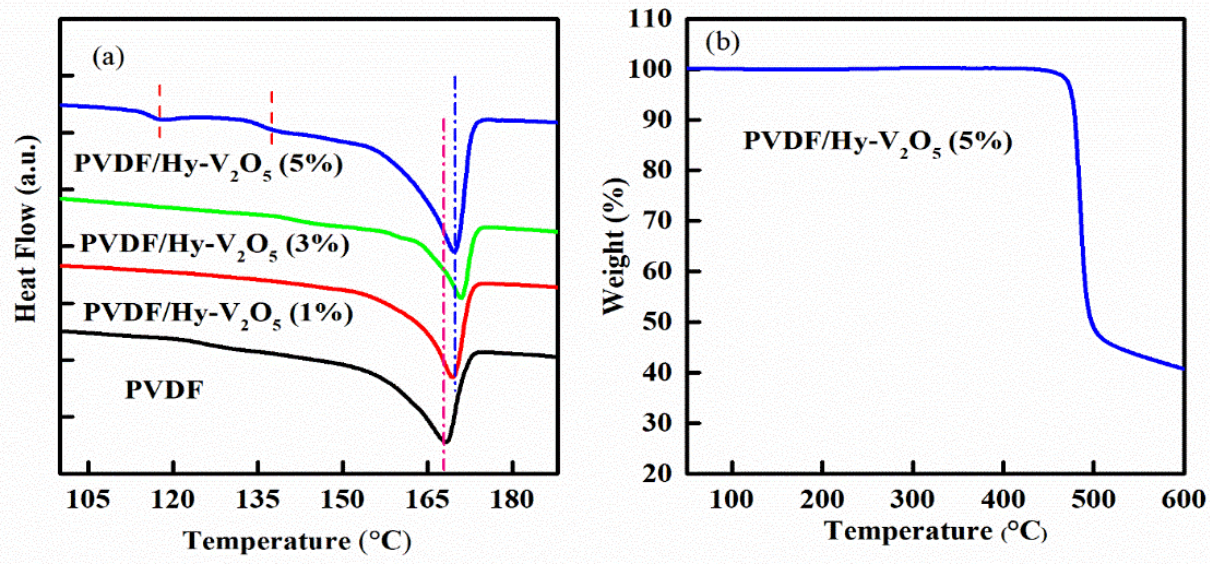

Figure 3.6. (a) DSC of pure PVDF and all compositions of PVDF/Hy-V_2O_5 (b) TGA thermograph of PVDF/Hy-V_2O_5 (5%).

3.3.6 AFM micrograph analysis and roughness of film

Figure 3.7 shows the Atomic Force Microscopy (AFM) image of the PVDF and nanocomposite film with a 3D plot. We can observe the roughness of the film surface in Figure 3.7(a). For analytical analysis, we plotted the roughness characteristics as shown in the Figure 3.8(a) with the help of Nova Px 3.0.4 rev software. Pure PVDF appears rougher than PVDF-based nanocomposites**.** The roughness of the PVDF appears to be slightly higher in comparison to the nanocomposite film which may be due to the bigger spherulite formation in the PVDF. The spherulite size on the PVDF surface could be higher in comparison to composite since loading of the filler in PVDF helps in enhancement in the crystallinity of the film, as clearly observed by the DSC studies. As the crystallinity increases, the size of the spherulites decreases. More number of spherulites of lower sizes could be there as the rate of grain growth is lower than the rate of nucleation process [111]. Another reason of low roughness of nanocomposite can be due to partially hydrophilic nature of Hy-V_2O_5 which speeds up the exchange of solvent and non-solvent during the phase change [112,113]. The measured root mean square roughness **(R_{rms})** for PVDF is 9.079±0.5 nm and for PVDF/Hy-V_2O_5 (5%) is 8.588±0.5

nm, from the green line shown in the inset in the Figure 3.8(a, b). Considering the standard deviation of the 0.5 nm in the rms roughness, the values of roughness for pure PVDF and PVDF/Hy-V_2O_5 (5%) are almost comparable. The power spectral density (PSD) characterizes the degree to which elements of different spatial frequencies contribute to the surface structure, providing additional information regarding surface roughness. There is a comprehensive description of surface topography characterization using spectral analysis elsewhere [114]. The isotropic PSD of the AFM image of pure PVDF and nanocomposite has been plotted with the help of Nova Px 3.0.4 rev software. Figure 3.8(c, d) shows the PSD with Hann windowing. The isotropic PSD in Figure 3.8(e) demonstrates that there is no preferred orientation of the surface features and that surface polymerization occurs without a preferred growth direction. The isotropic polymer growth mechanism for charge storage applications helps prevent charge leakage and thus improves charge storage duration. A synthetic scheme that produces isotropic polymer growth is preferable if charge storage rather than transport is the desired polymer functionality [52].

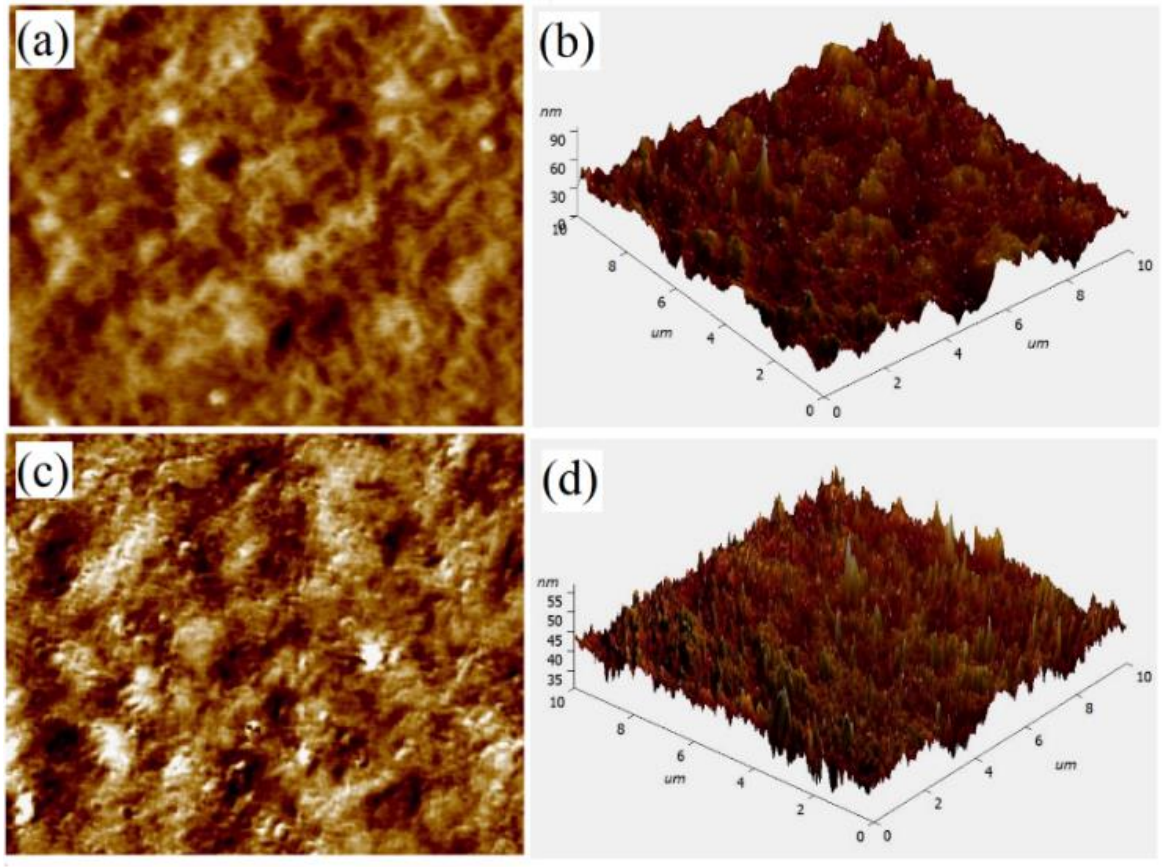

Figure 3.7. (a) AFM micrograph (10x10µm) of Pure PVDF, (b) 3D AFM micrographs (10x10µm) of Pure PVDF, (c) AFM micrograph (10x10µm) of PVDF/Hy-V_2O_5 (5%) and (d) 3D AFM micrographs (10x10µm) of PVDF/Hy-V_2O_5 (5%).

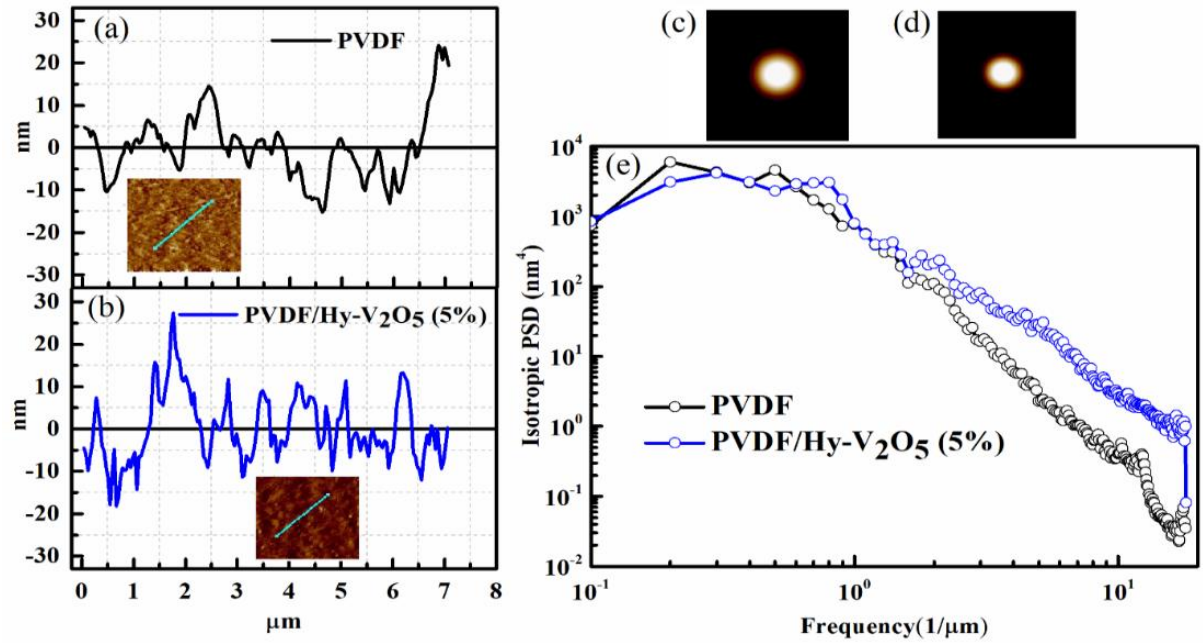

Figure 3.8. Roughness profile of (a) pure PVDF, (b) PVDF/Hy-V_2O_5 (5%). Hann Windowing of AFM micrograph for (c) pure PVDF and (d) PVDF/Hy-V_2O_5 (5%). (e) Isotropic 2D PSD Plot of PVDF and PVDF/Hy-V_2O_5 (5%).

3.3.7 Morphological analysis

Figure 3.9(a) shows the micrograph of Hy-V_2O_5 nano powder with the average primary particle size of 77.26 nm and particles seen in bigger size are agglomerated smaller particles. In Figure 3.9(b), histogram is plotted with the gaussian fit showing the average size of particles of Hy-V_2O_5 nano powder. In Figure 3.9(c), spherulites can be seen in pure PVDF film. The micrographs in Figure 3.9(d-f), reveal that as the Hy-V_2O_5 nanoparticles are loaded to the PVDF matrix, the spherulite size is decreased and difficult to resolve, which are clearly observable in the Figure 3.9(c) for pure PVDF. Further, loading of 5%vol filler may have increased the nucleation process as compared to the grain growth process because the nanofiller can work as the nucleation sites that leads to the invisible smaller spherulite in more numbers making it smoother[111]. As seen in Figure 3.9(f), there may be partial agglomeration of the V_2O_5 filler nanoparticles due to hydroxylation. To investigate if the agglomeration is present in bulk sample or just at the surface, the fractured cross section of nanocomposite films was imaged and its zoomed-out cross-section are shown in Figure 3.9(g-h). The Figure 3.9 (h), reveals that the particles are homogenously distributed in the bulk volume of the film with very minor agglomeration of some particles. Further, it can be concluded that the top surface of nanocomposite film is totally homogeneous even for higher loading of filler (5%vol). and there are no cracks or visible grains.

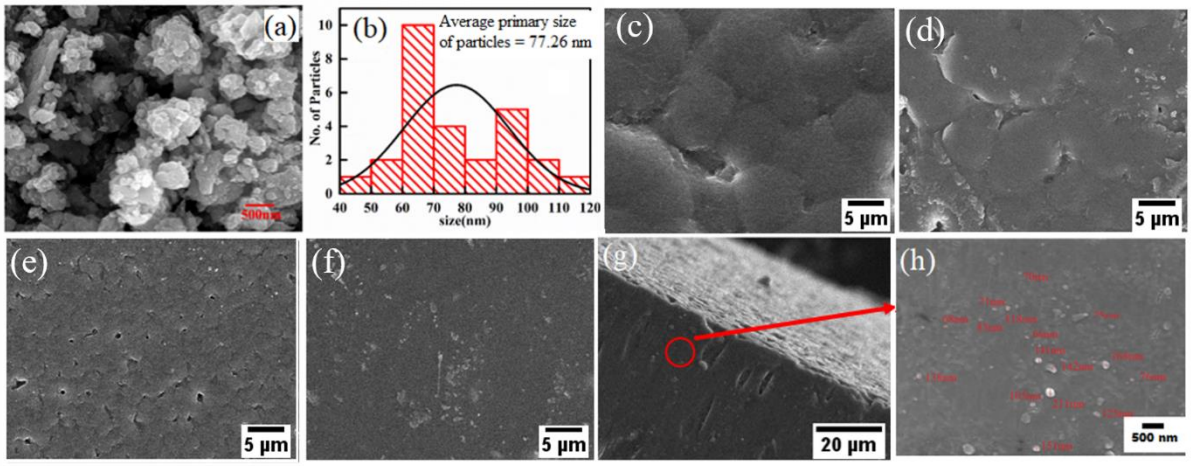

Figure 3.9. SEM micro-topographies of (a) Hy-V_2O_5 nanoparticles, (b) Histogram of the particle sizes of Hy-V_2O_5 (c) pure PVDF, (d) PVDF/Hy-V_2O_5 (1%), (e) PVDF/Hy-V_2O_5 (3%), (f) PVDF/Hy-V_2O_5 (5%), (g) Cross section of the nanocomposite film (PVDF/Hy-V_2O_5 (5%)), (h) Zoomed area of cross section of nanocomposite film.

We can observe some potholes in PVDF and PVDF/Hy-V_2O_5 nanocomposite films in Fig 7 (c-d). It is due to the bubbles between the glass and the films while preparing it. These potholes may have resulted in a decline in mechanical strength as well as in the electric breakdown strength of films [115].

3.3.8 Dielectric properties

The dielectric constant and loss were measured with respect to frequency and temperature and can be seen in Figure 3.10. The dielectric constant vs temperature plots were recorded at a frequency of 10^3 Hz. It can be observed that the dielectric constant of PVDF/Hy-V_2O_5 composites is increasing with the increment in the volume fraction of Hy-V_2O_5. At higher temperatures, the dielectric constant increases. The dielectric constant for the pure PVDF in our case is around 9, which can be matched with previous research [116] and for PVDF-Hy-V_2O_5 (5%), it is ~30 (29.86) at a frequency of 10^3 Hz, that is much higher than the pure PVDF. Such an increment in dielectric constant is credited to the gradual increase in interfacial space charge polarization between the polymer matrix and the filler. According to the Maxwell Wagner-

Sillars (MWS) effect that appears in heterogeneous systems having different dielectric materials, the addition of Hy-V_2O_5 to the PVDF/Hy-V_2O_5 composite adds more polarization groups that cause extra polarization under the application of an electrical field [117,118].

The Hy-V_2O_5 nanoparticles have large specific surface area ratio which creates namouras sites which are helpful in MWS effect. The dielectric loss is increased with the addition of Hy-V_2O_5 filler, but at lower loading of the filler, the loss is almost equal to the pure PVDF and even lower at higher frequencies and temperature. This is because of the fact that the p-type semiconducting Hy-V_2O_5 [93] with lower amount of holes at small filler loading may make dipoles with the negative charges of electronegative fluorine from the PVDF matrix to get neutralized. Further, it also can be attributed to the increment in dielectric constant at higher temperature than 80°C for low filler loading as Gouy-Chapman-Stern layer is maintained [6,92,119,120]. As the loading increases, the number of holes present at interface become higher than the negative charge present due to electronegativity of Fluorine in PVDF causing more loss at higher temperature. Figure 3.10(b) shows that the dielectric loss is decreasing with increasing frequency in the range 10^3 -10^5 Hz and then get increased up to 10^6 Hz. This increment is attributed to α_a relaxation which is associated with the glass transition of the PVDF polymer[121]. The PVDF's glass transition temperature has been shown to have a direct correlation to the loss peak, which is a dielectric manifestation of the micro-Brownian cooperative movements [121].

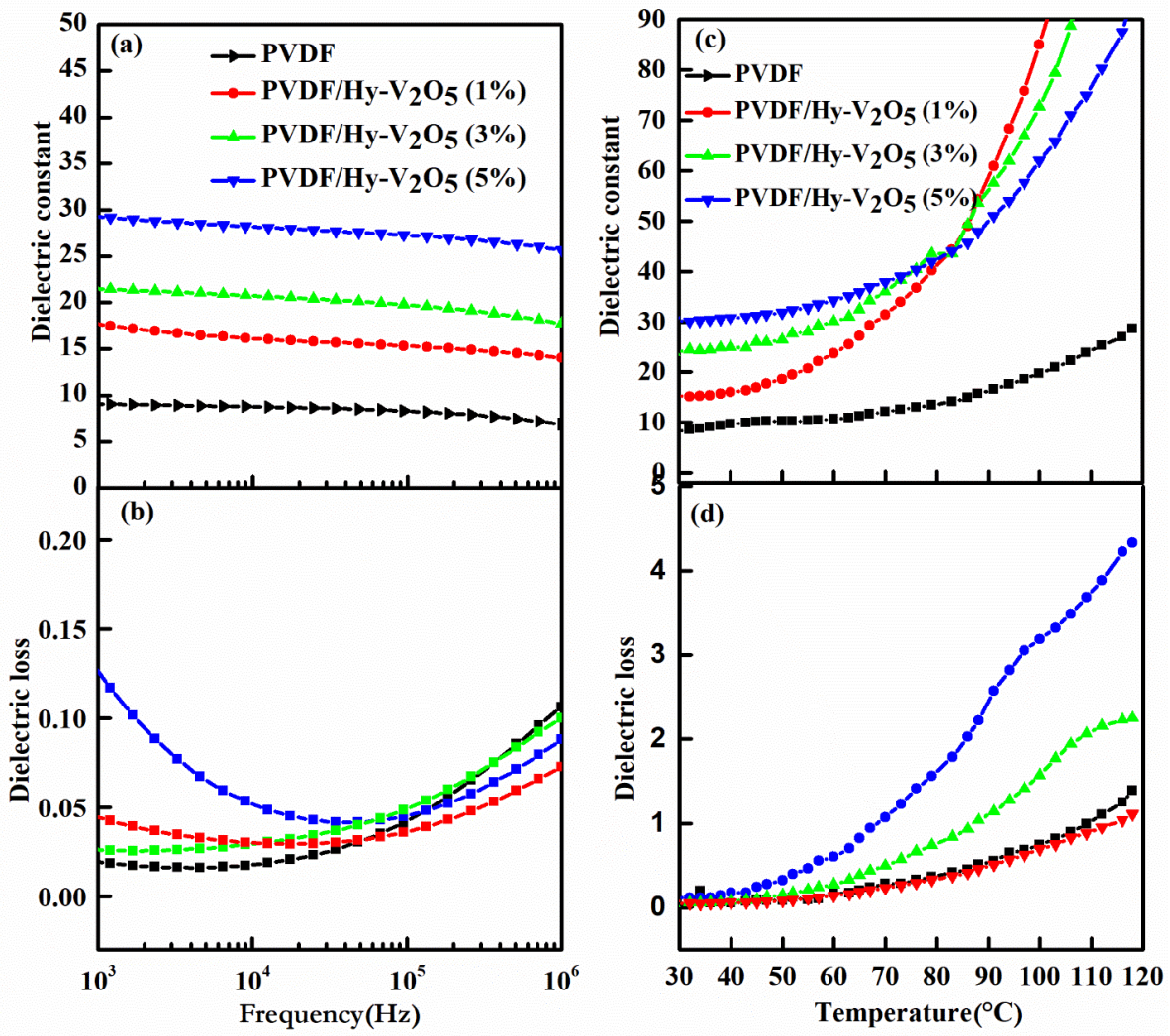

Figure 3.10. Dependence of dielectric constant and dielectric loss on frequency (a), (b); and temperature (c), (d) for pure PVDF and PVDF/Hy-V_2O_5 nanocomposite films with different compositions.

3.3.9 Ferroelectric P-E loop analysis

The polarization(P)-Electric field(E) hysteresis loop was measured for all vol% of fillers loadings as reinforcement in PVDF matrix, to calculate the energy density of PVDF based nanocomposite materials. The polarization in ferroelectric materials doesn't depend linearly on applied electric field. To determine the relationship between the polarization and electrical field for them, the Sawyer-Tower circuit is used. The P-E loop measured at electric field of 1000kV/cm and 10Hz frequency is shown in Figure 3.11 (c). We can see that addition

of filler resulted in increment in polarization. With 5% addition of filler the maximum polarization (P_{max}) is 2.7 μC/cm^2, which is more than 3 times of pure PVDF (P_{max} = 0.86 μC/cm^2) film and remanent polarization has also increased significantly from 0.25 μC/cm^2 for pure PVDF to 0.78 μC/cm^2 for PVDF/Hy-V_2O_5 (5%). This enhancement in the polarization is due to interfacial interaction of PVDF and Hy-V_2O_5. The interfacial interaction leads to electroactive phase increment in PVDF which causes the increment in the overall polarization[122]. Figure 3.11(a, b) show the schematic diagram of PVDF and nanocomposite film under the application of the electric field.

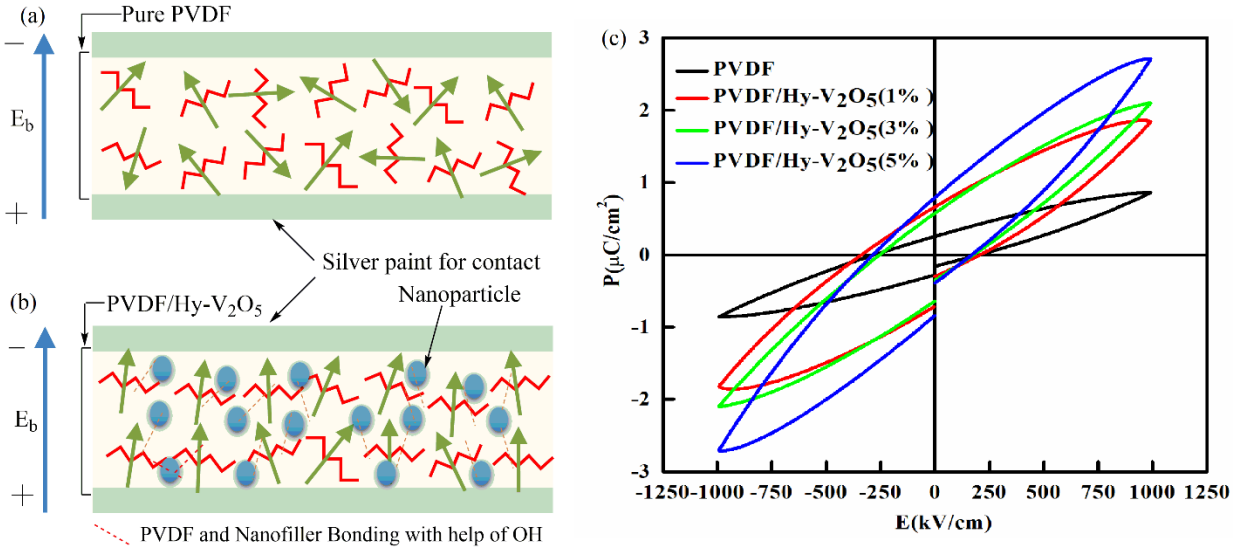

Figure 3.11. Schematic diagram of dipoles under applied field for (a) pure PVDF film, (b) PVDF/Hy-V_2O_5 film and (c) Ferroelectric P-E loops of PVDF and PVDF/Hy-V_2O_5 nanocomposite films with different compositions at 1000kV/cm, 10Hz frequency.

3.3.10 Breakdown strength and energy density using Weibull analysis

The energy storage density of a dielectric material is calculated using electrical breakdown strength, considering the linear system. The breakdown strength is calculated using the two-parameter Weibull cumulative probability function. The breakdown strength analysis is done with the help of the Weibull cumulative probability function given by the equation (1.17) as below [68].

$$P(E) = 1 - exp\left[-\left(\frac{E}{E_b}\right)^{\beta}\right]$$

where *P(E)* is the cumulative prospect of electrical breakdown, E is the actual breakdown field, E_b is the breakdown field when the cumulative prospect is 63.2%, and β is the shape parameter obtained by linear fitting, higher β represents the better results in this analysis. The equation used for this purpose are given as follow in equation (1.18) and (1.19) respectively [68].

$$X_i = \ln (E_i)$$

$$Y_i = \ln \left[-\ln\left(1 - \frac{i}{n+1}\right)\right]$$

Where X_i and Y_i represents the Weibull distribution function parameters, i is the consecutive number of sample and n represents the total number of samples. E_i is experimentally measured specific breakdown strength of specimen. X_i and Y_i should be in linear relationship while *β*, the shape parameter is the slope of line for the sample. The value of β is appropriately higher. Figure 3.12(a) shows the breakdown strength of samples with different colors for different percentages of filler loading in the polymer matrix. The breakdown strength has decreased slightly, as shown in Figure 3.12(b), and this trend has continued as the filler loading volume increases. This is due to the increase of agglomeration and defects in nanocomposite films with the increasing loading vol% of filler as evidenced by the HR-SEM images [123]. The electrical breakdown take place in materials where the area is prone to leakage current. Another cause of the reduction in the breakdown strength of nanocomposites is that, introduction of a material as reinforcement with a different dielectric constant to a polymer matrix leads to a highly inhomogeneous electric field around it[124]. The breakdown strength (E_b) and shape parameter (β) were 2208 kV/cm and 12.18 for the pure PVDF film. As the 1% Hy-V_2O_5 is loaded to the PVDF matrix, E_b was found to be 1900.74 kV/cm and β was 9.3. With further increment in vol % of filler up to 3% and 5%, E_b was recorded as 1797.22 kV/cm and 1766.93 kV/cm, the value

of shape parameter was found to be 13.07 and 9.37 respectively. The energy density of nanocomposites was calculated using the given equation 5, that is applicable for the linear dielectrics. We used this method to compute energy density in order to get a sense of the variation in energy density with composition, at the maximum electric field before its breakdown occurs, because we were unable to measure the ferroelectric loop till breakdown strength value due to the large thickness of sample and limitation of our system application (0 to 10kV). The energy density has been calculated by the given equation (1.20).

$$\text{Energy density (U)} = \frac{1}{2}\varepsilon_r\varepsilon_0 E_b^2$$

where $\varepsilon_r, \varepsilon_0$ is dielectric constant of nanocomposites and vacuum and E_b is the breakdown strength of material. The high energy discharge efficiency and high energy density, both are desired for the better performance of a dielectric material for the application in high energy density storage capacitors. PVDF's energy density was calculated to be 1.94 J/cm^3. Figure10(b) shows that the addition of filler as reinforcement improved the energy storage density almost by more than 2 times (4.68 J/cm^3) with 5 vol % loading.

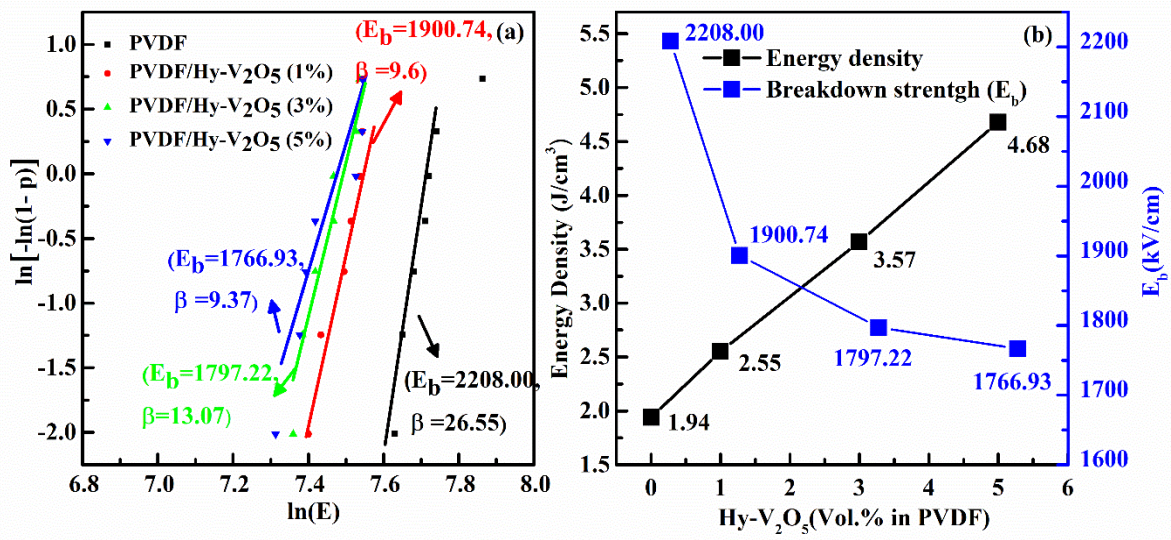

Figure 3.12 (a) Plot of Weibull distribution function parameters and (b) Energy density and Breakdown strength (E_b) of PVDF and PVDF/Hy-V_2O_5 films with different compositions.

3.3.11 Energy density and discharge efficiency from P-E loop

The charging and discharging paths are not coincident due to hysteresis in P-E loops so energy delivered to the capacitor cannot be released completely. The energy discharge efficiency or energy efficiency (η), energy discharge density or energy density ($\boldsymbol{U_d}$) and energy loss density($\boldsymbol{U_l}$) can be calculated using the equations (1.11), (1.12) and (1.13). The Figure 3.13 (b) shows, the energy density and energy efficiency as calculated using the given equations (1.11 to 1.13) from the ferroelectric polarization vs electric field loop[10].

where, Energy discharge density (U_d) = $\int_{P_r}^{P_{max}} Edp$

$$\text{Loss}(U_l) = \int_0^{P_{max}} Edp - \int_{P_r}^{P_{max}} Edp$$

$$\text{Energy efficiency } (\eta\%) = \frac{U_d}{U_d+U_l} \text{ x } 100$$

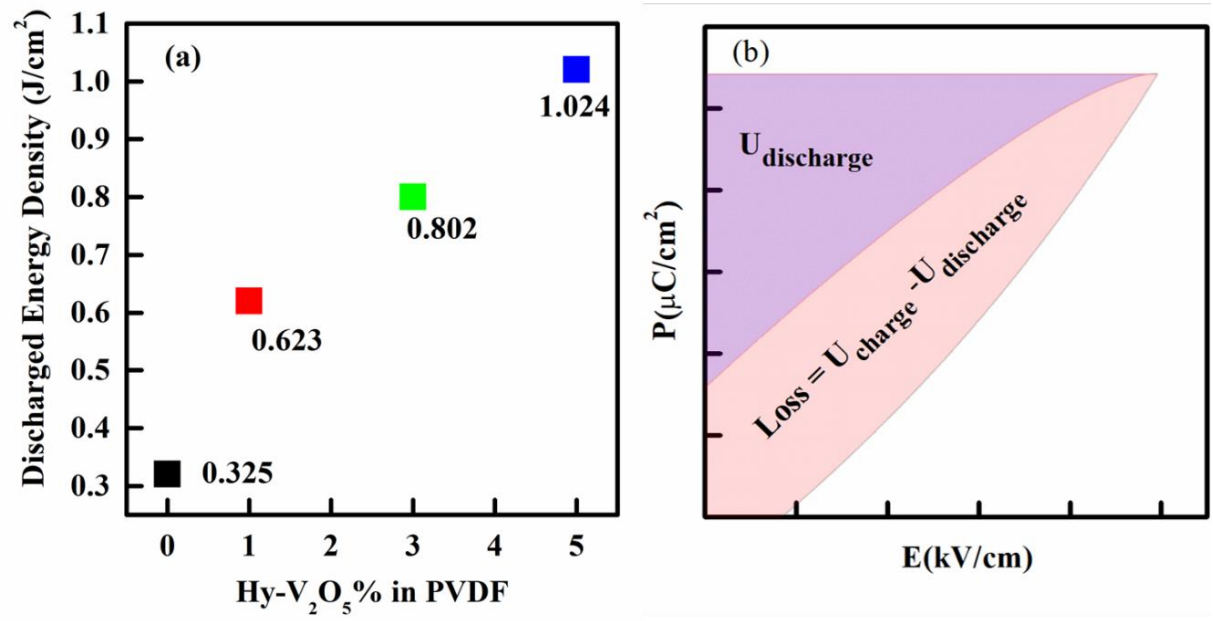

Figure 3.13 (a) Discharged energy density (U_d) (b) Schematic diagram for calculation of Energy storage efficiency.

Where, E is applied electric field and P_r is the remanent polarization, P_{max} is the maximum polarization with respect to maximum experimental electrical field. Energy loss density is caused by the ferroelectric domain reorientation. The calculated discharge energy

efficiency, with the help of Figure 3.13(b) and equation 6, for the 5vol% filler is 60.59% that makes our dielectric nanocomposite film very suitable for the application as the high-performance flexible energy storage devices having sufficient energy density, breakdown strength and thermal stability. Table 3.1 compares the results of previous research work and our work for discharged energy density (U_d), the energy efficiency (η) with electric field (E) (at which U_d and η are calculated) and dielectric constant (ε_r). The comparison of electrical field strength (E_b), energy efficiency (η) and discharged energy density (U_d) obtained in this work with previous literature further implies that we have got better results for the application discussed above.

Table 3.1. Comparison of the performance of earlier reported systems with our nanocomposite**.**

Sample	**U_d (J/cm^3)**	**(η%)**	**E (kV/cm)**	**ε_r**	**Reference**
PVDF/Ag(1%vol)@$BaTiO_3$ (20%vol)	0.83	~45	600	20	[125]
PVDF/TiO_x (1%wt)	7.43	~55	4800	22	[10]
PVDF/ H_2O_2-DN-101-$BaTiO_3$ (10%vol)	4.3	~48.0	2400	~21	[126]
(26.0%Vol) h-BN-RGO-epoxy	0.51	77.0	1000	~11	[127]
(1%wt) rGO-Ag/PVDF	0.26	--	150	-	[128]
PVDF/ Hydroxylated $BiFeO_3$ (7%wt)	0.15	--	14	~15	[73]
PVDF/$LaFeO_3$ (15%wt)	--	--	--	~8.5	[129]

PVDF/Hy-V_2O_5 (5%vol)	1.02	60.59	1000	29.86	This work

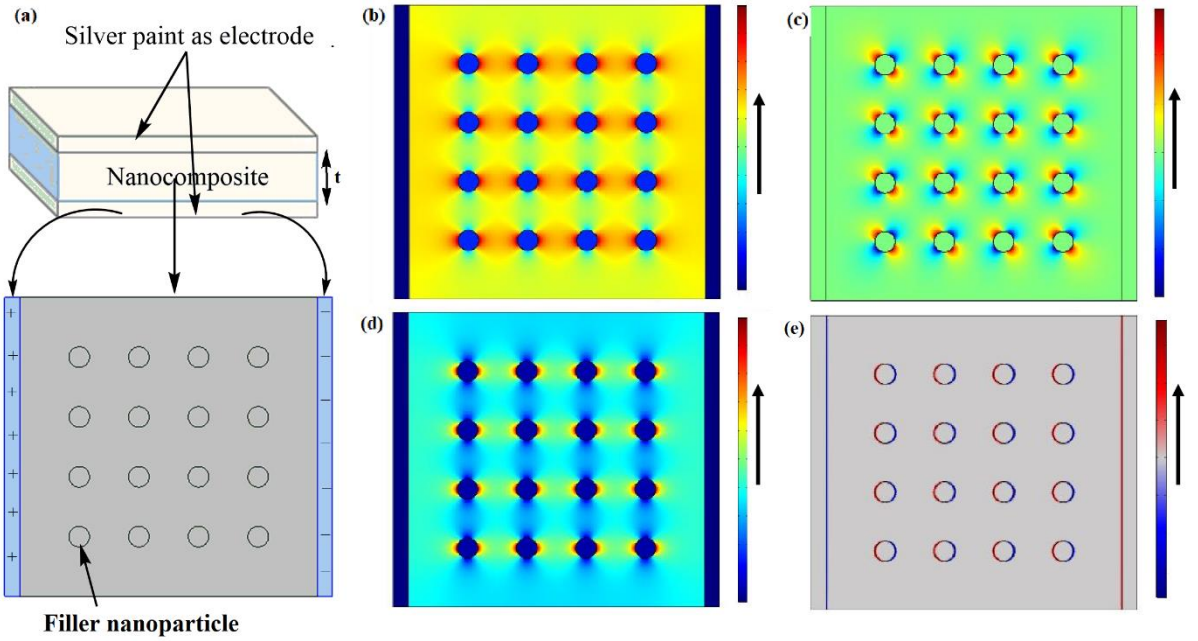

Figure 3.14 (a) Schematic and 2D simulation of Nanocomposite, (b) Electric displacement field, (c) Electric field, (d) Energy density and (e) Space charge density.

To mimic, visualization and the distribution of electrical field, energy density, electric displacement field and space charge density as flexible capacitor of the flexible nanocomposite film, we carried out the 2D simulation of nanocomposite with the help of COMSOL Multiphysics 5.5 as shown in the Figure 3.14. The 2D simulation model is of cross section of the capacitors flexible film as shown in the Figure 3.14(a) with the silver paint electrode. Figure 3.14(b) shows the electric displacement field of the nanocomposite films. The electric field shown in Figure 3.14(c) depicts that after a limit of applied electric field, a path around the nanofiller may be created easily. Figure 3.14(d) visualizes the charge accumulation around the filler and associated energy density. Figure 3.14(e) shows the space charge density in the nanocomposite film that can be helpful in understanding and visualizing the space charge polarization which is an important reason of enhancement the dielectric and storage properties.

3.4 Theoretical analysis of percolation and interface thickness.

We have already discussed the percolation phenomena in the section 1.4 of Chapter 1, when the nanoparticles are reinforced in the polymer matrix the Interface is formed around the nanoparticle of the filler inside the PVDF matrix with a certain thickness depending on the charge accumulation around the nanoparticle. Gouy chapman-stern layer or double layer model used to the thickness of the interface, this is actually Debye length. Debye length of the system has been calculated with the help of equation (1.15) as given the Chapter 1. The inter filler distance has been calculated using the equation (1.16). The average nanoparticle size of the V_2O_5 is around ~78nm as shown in the FESEM micrographs as shown in the Figure 3.9. The measured dielectric constant of the bulk V_2O_5 is ~4.6, it is used to calculate the Debye length, The charge density is 0.59×10^{15} /cm^3 [130], thus the Debye length (L_d) estimated is ~106nm. The calculation of the inter-filler distance of the filler particles in the PVDF matrix, was measured surface to surface, it was found to be ~ 95 nm when the filler loading was 5 vol%. Because the δ_i is comparable to the L_d for the 5vol% loading of the Hy-V_2O_5 in the PVDF loading, we can say that it is the critical volume% or the percolation threshold for the filler loading in PVDF matrix. If the nanocomposite is loaded more than this amount, it will be susceptible to low dielectric strength and have a lower polarisation value as there can higher numbers of the conducting path in the matrix. Keeping in mind of all discussed above, the 8vol% loading of the filler in PVDF has not been considered for the characterization/investigation or usable for application purpose. Still, we have performed the PE hysteresis loop measurement.

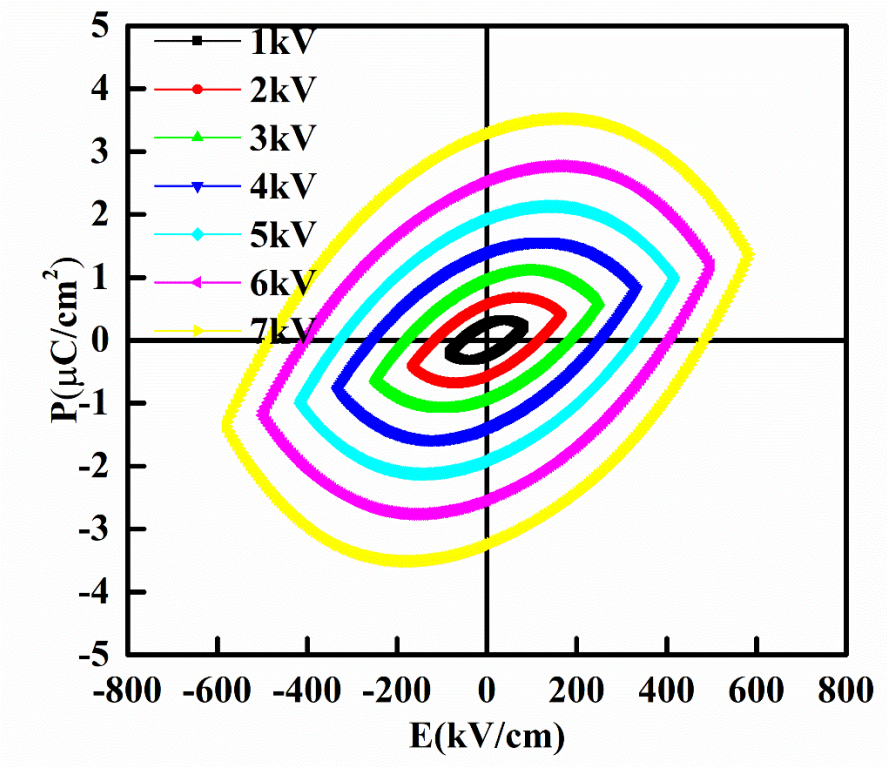

Figure 3.15. PE Loop of the PVDF/Hy-V_2O_5 (8%).

The PE loop for the 8 vol% loading the PVDF matric is shown in the Figure 3.15. The PE loop seems to be round in nature that's this type of loop shows the higher loss and increased conductivity of the nanocomposite film. Thus, It can be said that above 8 vol% loading, the percolation occurs and the film becomes partially conducting after applying higher electric field or breakdown occurs at early stage of electric field as compare to lower loading of the filler.

3.5 Conclusions

A facile solution cast method was used to synthesize the PVDF/Hy-V_2O_5 based flexible nanocomposite films with varied concentration of the filler. The effects of Hy-V_2O_5 filler on the dielectric property, phase structure, and energy storage density of nanocomposite films were discussed in detail. The DSC helped in the phase identification of PVDF and nanocomposite films. The XPS analysis is done to ascertain the presence of nanofiller in the

nanocomposite. The energy storage phenomena were studied in depth using AFM micrographs and an isotropic PSD profile. The enhancement in the dielectric constant from ~9 (pure PVDF) to 29.86, and the maximum discharge energy storage density from 0.32 (pure PVDF) to 1.024 J/cm^3 (220% increment) was obtained at a low amount of the filler (just 5vol% of Hy-V_2O_5) in the PVDF matrix, which resulted in maintaining the breakdown strength to 1766.93 kV/cm. The overall work shows better improvement in the properties of PVDF film with the addition of semiconducting Hy-V_2O_5 making this nanocomposite applicable in flexible energy storage film.